EPMA, micro-PIXE, synchrotron microprobe and TEM study of visible and invisible accumulations of Au and PGE in black shale and organic matrix, Kupferschiefer, Poland

H. KUCHA

Institute of Geology and Mineral Deposits, 30-059 Krakow, Avenue Mickiewicza 30, Poland

W. PRZYBLOWICZ, M. LANKOSZ

Institute of Physics and Nuclear Techniques, 30-059 Krakow, Avenue Mickiewicza 30, Poland

F. VAN LANGEVELDE

Department of Physics and Astronomy, Free University, 1081 HV, Amsterdam, The Netherlands

AND

K. TRAXEL

Physikalisches Institut der Unviersität Heidelberg, D-6900 Heidelberg 1, Germany

Abstract

The Kupferschiefer contains from 0.3 to 30 wt.% of organic matter, with an average value close to 10 wt.%. The concentration of heavy metals increases strongly towards the base of a black shale horizon. Where the black shale rests directly on red sandstone, the bottom few mm of the shale may contain (ppm): Hg 8–1500, mean 174; Ag 310–5780, mean 1222; Au 1–3000, mean 40; Pd 2–1000, mean 37; Pt 2–340, mean 18. The shale, enriched in noble metals, is overlain by thucholite shale. The flotation sulphide concentrate contains 1–3 ppm Au and a detectable Pd and Pt content. Selected gravity concentrates from the black shale contain 4–56 ppm Au, up to 25 ppm Pd, while the Pt content does not exceed 1 ppm. A tightly intermixed clay–organic matrix of the noble metal-bearing shale contains small accumulations of Au, Pt and Pd presumably as organometallic compounds.

Thucholite is present locally. It contains inclusions of uraninite, brannerite and noble metal minerals lcoated at the boundary between optically isotropic and anisotropic components. The optically homogeneous organic matrix of the thucholite contains discrete inclusions of UO_2, brannerite, electrum and organic compounds of Au, U, Pt and Ni varying in size from 0.008 to 0.025 μm as shown by TEM. Gold occurs in a continuous Au–Ag series. Refractory Au is present as substitutions in native silver and in the organic matrix of the shale and thucholite. Palladium forms several arsenides and sulphoarsenides. Refractory Pd is present as substitutions in Ni–Co arsenides and in the organic matrix of the shale and thucholite. Platinum is present as substitutions in the organic matrix of the noble-metal-bearing shale and thucholite.

The average detection limits of micro-PIXE were 8–10 ppm, and those of the SXRFA from one to a few ppm. A major factor defining detection limits in the studied samples were minor uranium lines overlapping spectral lines of the studied elements.

KEYWORDS: noble metals, organometallic compounds, thucholite, Kupferschiefer, Lubin, Poland.

Introduction

FIVE mines, Lubin, Polkowice, Rudna, Sieroszowice and Malomice (Fig. 1) work the Kupferschiefer and produce about 300 000 T Cu, 12000–14000 T Pb, 700–900 T Ag, 280 T Ni and *c.* 0.35 T Au per annum. Recently, 75% of the gold has come from the Polkowice mine alone. Some Pt

Mineralogical Magazine, March 1993, Vol. 57, pp. 103–112

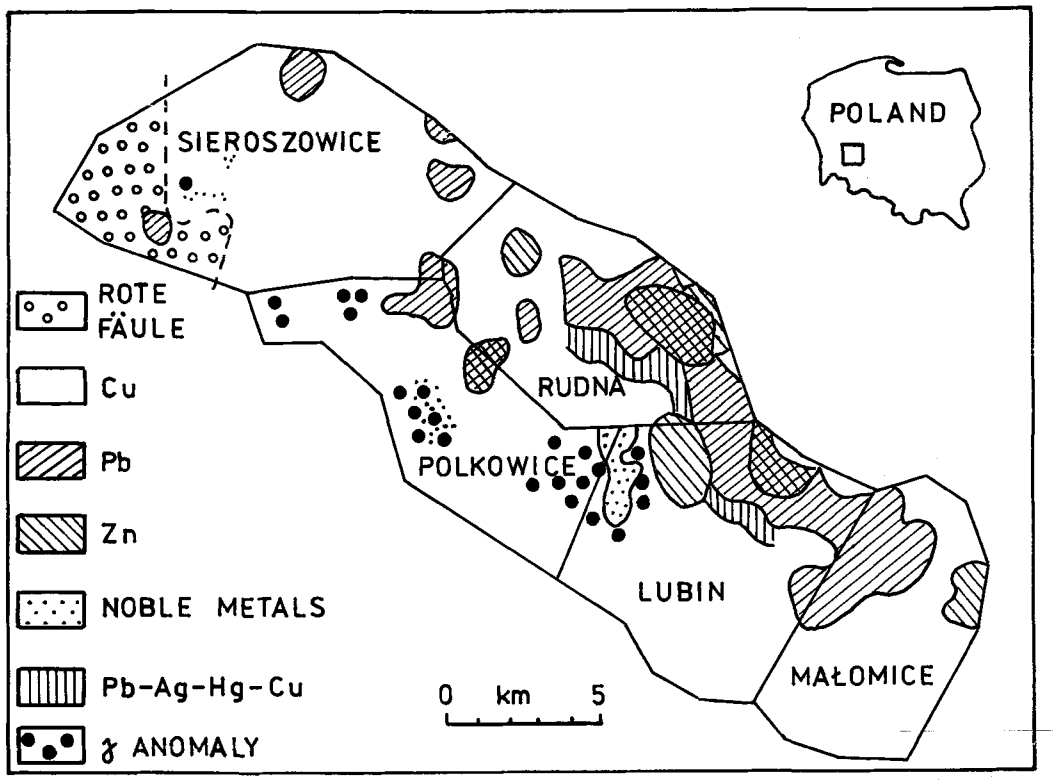

FIG. 1. A general map of Lubin mining district.

and Pd are also recovered; however, recent estimations suggest that recovery of noble metals does not exceed *c.* 25%. This is connected with the applied mineral processing techniques used—flotation gives a very poor recovery of native metals. Quantities of V, Mo and Co in the ore are similar to those of Ag but none of these metals is recovered on the industrial scale.

The flotation sulphide concentrates have a detectable Pd and Pt content and contain Au values grouped close to 3 ppm from the Polkowice mine, while the concentrate from other mines shows Au concentrations close to 1 ppm (Table 1).

Materials and methods of investigation

This study is based on 300 samples collected in gold-bearing areas in the Lubin, Polkowice, and Sieroszowice mines.

Electron probe microanalyses (EPMA) were made with an ARL SEMQ probe at the Mining University, Leoben, Austria. The following conditions were applied: accelerating voltage 20 and 25 kV, beam current 150 μA, sample current measured on brass 15 nA, time counting for noble metals including Ag was 40 sec, time counting for other elements was 10 sec. The following standards and spectral lines were used: S-Kα and Fe-Kα (FeS_2), Cl-Kα (tugtupite), Si-Kα (SiO_2), Ti-Kα, Ni-Kα, Co-Kα, Cu-Kα and Lα, Pd-Lα, Ag-Lα, Pt-Lα, Au-Lα, U-Lα. All measurements were ZAF corrected.

The PIXE analyses were carried out in the Laboratory of Applied Nuclear Spectroscopy, Institute of Nuclear Physics in Krakow. The proton energy was *c.* 2.6 MeV; the beam diameter on target was 3 mm with the possibility of focusing a beam on the selected area of the sample. Two multielement standards made by the International Atomic Energy Agency SOIL-5 and SOIL-7 were used. Induced X-rays were measured with the ORTEC Si(Li) semiconductor detector with resolution *c.* 200 eV. The data reduction was performed with a software package developed for thick target analysis (Kajfosz, 1987; Kajfosz and Kwiatek, 1987).

Recent progress in micro-PIXE (MPIXE) methodology made analyses of thick targets of the

TABLE 1. The content of noble metals in selected areas of black shale and in some mineral processing products. Upper figure - range; lower figure - average. Ag to Pd in ppm, Rh in ppb.

AREA	Ag	Au	Pt	Pd	Rh	(N)
Lubin West	310-5780	1 -3000	2 -340	2 -1000		31
Polkowice East	1222	40	18	37		
Polkowice	265-3080	1 - 115	0.01- 3	1 - 15	1 -52	5
Central	856	24	0.3	3	9	
Sieroszowice	117-3991	0.01- 13	0.01- 1	0.10- 2	2 -45	8
	518	5	0.2	0.42	12	
Flotation		1.74- 2.1	0.05- 0.16	0.07- 0.14	2.5-53	4
concentrate		2.00	0.09	0.12	22	
Polkowice						
Gravity		4.0 - 56	0.10- 0.81	0.10- 25	5.0-84	5
concentrate		17	0.42	4.91	32	
Polkowice						

N - number of analyses

same type as those used in EPMA analyses possible (Campbell *et al.*, 1984, 1988). Several applications have already been reported, and detection limits obtained with MPIXE are 3 to 30 times better than corresponding detection limits of EPMA (Remond *et al.*, 1987). MPIXE analyses were made at the Max Planck Institut für Kernphysik in Heidelberg, Germany, using the same analytical points as those used in EPMA measurements. The proton beam current of the mesured black shale matrix and thucholite ranged from 45 to 450 pA. The data acquisition time was 10–20 min. A 195 μm thick aluminium absorber was placed between the target and Si(Li) detector. The resolution of the detector at 6.4 keV was *c.* 170 eV. Emission spectra were processed using the least-squares method of Kajfosz (1987) with backgrounds cut using nonpolynomial approximation (Kajfosz and Kwiatek, 1987). 30 EPMA measurements were used to calibrate against an internal Fe standard. The depth of effective proton penetration in the thucholite matrix was up to 100 μm and in the black shale matrix up to 70 μm (Przybylowicz *et al.*, 1990).

Synchrotron X-ray fluorescence analysis (SXRFA) was made with a synchrotron microprobe at Daresbury, U.K. The following experimental conditions were used: beam energy of 15 keV, energy bandwidth about 0.3 keV, and beam spot size 15 × 20 μm on target. For the thucholite matrix, 95% of the fluorescence for Fe-Kα was calculated to come from the upper 100 μm layer (Kopp *et al.*, 1990). Acquisition time per point was 200 s for the studied thucholite (Przybylowicz *et al.*, 1992).

Atomic absorption spectrometry (AAS) mesurements were made at the Institute of Geology, Leoben, Austria. The sample decomposition procedure was similar to that used in a former study (Kucha, 1990). Au, Pt, Pd and Rh were collected on the tellurium trap. Transmitted electron microscopy (TEM) was conducted at 100 kV using a Jeol JEM 100C microscope supplied with an EDS detector. Particles for TEM were collected from areas previously analysed with EPMA.

The shale

The 0 to 1 m thick black shale either directly overlies white sandstone or is separated from it by a dolomite bed 0 to 20 cm thick. The shale may be absent locally and an organogenic limestone (dolomite) occurs instead. The main minerals of the black shale are illite, glauconite, carbonates, detrital and secondary overgrown quartz, phengite and 0.3 to 30 wt.% of organic matter. The shale contains much higher amounts of major and associated metals than the underlying sandstone or overlying dark dolomite and the vertical distribution of metals in the black shale is not homogeneous, reaching peak values at the base, where the Cu content is up to 39.1 wt.%, V, Mo, Ni, Co, As and Ag may reach 5000 ppm (Kucha, 1976; Salamon, 1979; Kucha *et al.*, 1983) and U may reach 163 ppm (Piestrzynski, 1990). The

shale is often referred to as copper-, lead-, zinc;, noble metal- or thucholite-bearing according to the dominant metal or mineral.

The black shale passes transitionally into overlying dark dolomite.

Noble metals

So called noble metal-bearing areas (Fig. 1) are defined as areas where the Au content in the bottom few mm of black shale is above 1 ppm (Kucha, 1990). There are three such areas:

1. The western part of Lubin and the eastern part of Polkowice mines. This Au-bearing area spatially overlaps the largest and most significant γ-anomaly in the mining district (Fig. 1). Noble metals are present in a few mm thick noble metal-bearing shale (Kucha, 1982, 1983) at the base of the black shale. The noble metal-bearing shale is directly overlain by 0 to 2 cm thick thucholite shale responsible for the extensive γ-anomaly. Gold is present usually where black shale rests directly on the red sandstone, i.e. in areas of the highest vertical redox gradient. These areas are marked also by increased radioactivity caused by an increased U content. In such areas, gold is present as a continuous Ag–Au series, as an admixture in Pd arsenides (Kucha, 1984), Ni–Co arsenides and in organic matter (Kucha, 1975, 1981, 1982, 1983). Pd is present in the form of several arsenides and sulpho-arsenides, as an admixture up to 5.5 wt.% in Ni; and Co-arsenides (Kucha, 1984) but it is also found in organic matter (Kucha, 1975, 1981, 1982). No individual minerals of Pt have been found so far. The Pt is present in organic matter (Kucha, 1982; Przybylowicz *et al.*, 1990).

2. The central part of Polkowice mine. In this area a γ-anomaly is also present, although it is not as extensive as in the former case (Fig. 1). White sandstone may be locally absent and black shale may rest directly on the red sandstone. Native gold was found in areas where a high Ag content coincides spatially with γ-radiation, and in areas where black shale contains centimetre-size lenses of red Fe–Ca phosphates. In the latter case native gold is associated with clausthalite, hematite, mooihoekite and haycockite. The silver content in the area is high (Table 1), but Pd and Pt are much lower. Five gravity concentrates obtained from the silver-rich shale show Au contents from 4 to 56 ppm, with an average value of 17 ppm. In contrast, the average flotation concentrate of Polkowice mine contains only 2 ppm of gold. The Au occurs mostly as a continuous Ag–Au series, but a few grains of unspecified Au tellurides were found in a gravity concentrate. Thucholite from the area usually contains small inclusions of gold.

3. Sieroszowice. In the Sieroszowice mine (Fig. 1) gold occurs within a narrow zone (belt?) parallel to and close to the boundary of the Rote Fäule. The zone was found in a few sampling profiles traversing the Rote Fäule–sulphide boundary. The highest Au content of 13 ppm was found in the very bottom of the black shale. Pt does not correlate with Au in vertical section. The decisive factor controlling distribution of gold here seems to be the Rote Fäule–sulphide boundary. This problem requires further study.

The black shale matrix

The noble metal-bearing shale matrix was studied by PIXE, MPIXE, EPMA and TEM.

The content of organic matter in the black shale varies from 0.3 to 30 wt.%. Extractable bitumens constitute no more than *c.* 1–2 wt.% of this. The rest is kerogen, closely intermixed with clay minerals forming a clay–organic matrix to the shale. The soluble bitumens contain significant amounts of V, Fe, Co, Ni, Cu, As and Mo, with V and Ni present as ethioporphyrins (Kucha *et al.*, 1983; Sawlowicz, 1985). The Cu, Mo and As content may be high in the soluble bitumens but no specific organic compounds of these elements have been identified.

Kerogen, obtained after extraction of soluble bitumens and removal of carbonates by HCl and clay minerals by HF treatment, is composed mainly of conjugated benzene rings (Kuch, 1976). CO, OH, CH_2 and CH_3 are bound directly to benzene rings or are incorporated in insoluble resins.

The black shale matrix contains ubiquitous μm-size graphite flakes oriented parallel to the bedding. TEM study shows that graphite and clay minerals (illite, montmorillonite) form syntaxial intergrowths (Kucha and Wierczorek, 1988). Aromatic hydrocarbons were epitaxially conjugated and oriented on the tetrahedral sheets of clay minerals thus forming tightly intergrown, immobile clay–organic matrix and true graphite in places. Montmorillonite and illite inclusions oriented parallel to the 001 plane of graphite are typical constituents of microscopically visible graphite–phyllosilicate sandwiches. Under TEM such sandwiches show characteristic stacking faults and dislocations caused by a small misfit of the graphite lattice and mica tetrahedral sheet. The c_o parameter of montmorillonite found in graphite–mica sandwiches is increased up to 2.240–2.480 ± 0.025 nm. This suggests that one phyllosilicate sheet is coordinated with a graphite

layer on both sides, where the tetrahedral sheets are avaialble (Kucha and Wieczorek, 1988).

A typical noble metal-bearing shale is a few mm thick and composed of an optically irresolvable clay–organic matrix enclosing detrital quartz grains, large lenses (to a few cm) of Ca-phosphates (Kucha, 1983), inclusions of ore mineral aggregates composed of native gold, covellite, Pd_3As_5, Ni- and Co-arsenides, castaingite and bisulphides (Fig. 2*a*). Under higher magnification μm-size inclusions of native gold, castaingite and TiO_2 may be recognised in the clay–organic matrix (Fig. 2*b*).

The clay–organic matrix of noble metal-bearing shale is enriched in U and noble metals (Table 2). Fe, Cu, As, Ti, V, U and NI may be considered as major metallic admixtures of the matrix (Table 2). Mo, Pd, Ag, Pt and Au should be regarded as traces. The results obtained with PIXE, MPIXE and EPMA (Table 2) show similar concentrations of major metals, especially when the metals are homgeneously distributed in the clay–organic matrix. The best examples are provided by Cu, As, Ni and Fe (Table 2). The values measured as traces, such as Pd, Ag, Pt and Au vary widely as regards the method of analysis (Table 2). Concerning Ag and Pt, the results are surprising, being detected by EPMA, but not by MPIXE despite the fact that the MPIXE detection limit of Ag is *c.* 15 times and Pt *c.* seven times better than the corresponding detection limits of EPMA (Table 2). However, the discrepancy is only apparent and is explained by the number of analyses, 56 EPMA and only 13 MPIXE determinations of the clay–organic matrix of the noble metal-bearing shale (Table 2). A detailed examination of the distribution of traces in the matrix indicates that 25 MPIXE measurement points

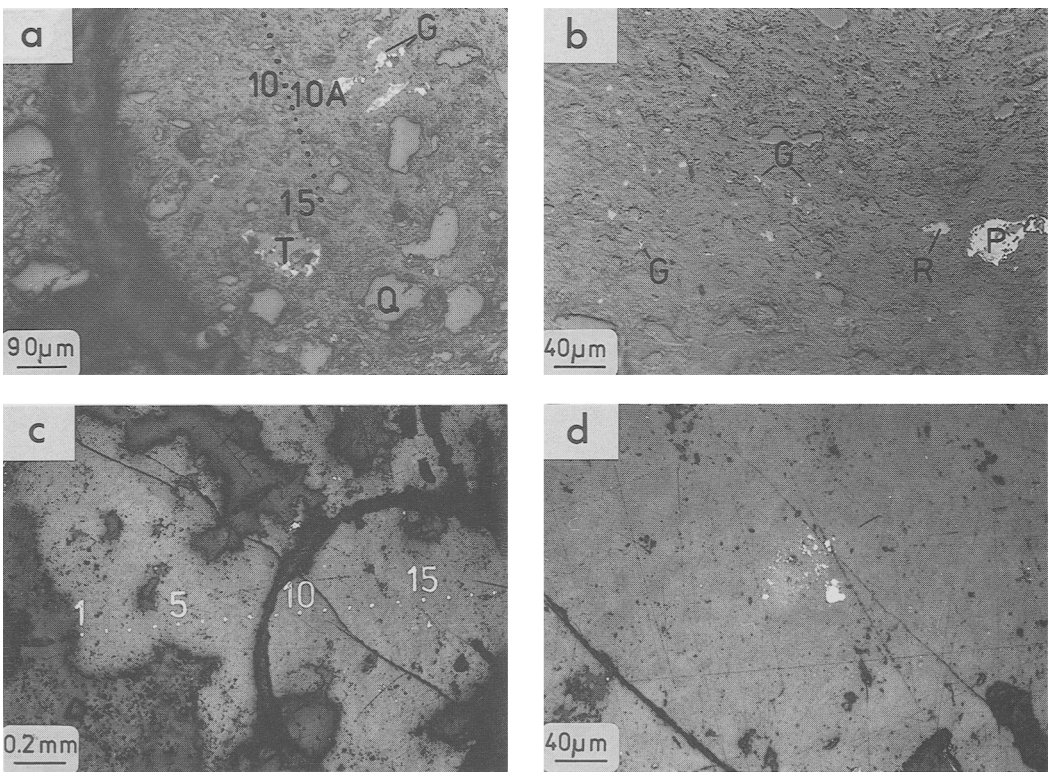

FIG. 2. (*a*) Photomicrograph of noble metal-bearing shale. Reflected light, sample 60G, Lubin mine. Arabic numerals denote EPMA and MPIXE profile. Q—quartz, T—thucholite, G—gold, white—unspecified Pd arsenides. (*b*) The clay–organic matrix of the noble metal-bearing shale with minute inclusions of electrum (G), rutile (R) and Pd-arsenide. Reflected light, sample 60G, Lubin mine. (*c*) Photomicrograph of thucholite grain surrounded by ferroan dolomite. Arabic numerals denote spots of SXRFA and EPMA analyses. Reflected light, sample 45C, Lubin mine. (*d*) Thucholite with dispersed minute inclusions of electrum (white). Electrum is present in anisotropic component B of thucholite. Reflected light, oil immersion, sample 45C, Lubin mine.

would be enough to detect Ag and Pt in the studied profile, and the expected average value should match that obtained by EPMA.

Relationships between elements in the studied clay–organic matrix are similar when studied by EPMA and MPIXE. The studied profile was set to avoid microscopically visible mineral inclusions (Fig. 2*a*). The observed Fe content (Table 2) may be entirely accommodated by clay minerals and organic matter. According to TEM study the clay–organic matrix is composed of illite (minor montmorillonite) flakes *c.* 1 μm in size embedded in an organic mass. For this reason the clay–organic matrix looks homogeneous when studied by MPIXE and EPMA. Ni is homogeneously distributed, except where it correlates with Cu, As and Co (Przybylowicz *et al.*, 1990) due to submicroscopic inclusions of cobaltite–gersdorffite and/or tennantite (Kucha, 1976). The remaining Ni is probably bound to pyrrole rings. Cu is homogeneously distributed in the matrix, except for micro-inclusions of sulpho-arsenides. Such a distribution pattern suggests that the basic portion of Cu in the clay–organic matrix may be bound to clay minerals (Kucha, 1985) and solid bitumens.

Sulpho-arsenide microinclusions also account for some As, but a majority of this element is homogeneously distributed, and probably bound to solid bitumens. This assumption may be supported by a high As content observed in the thucholite matrix (Kucha, 1982).

Pd and Pt were detected in three of 28 studied points. They do not correlate with other elements and may be bound to solid bitumens.

Au was detected in four points by EPMA and in two by MPIXE. In one of these microareas Au correlates with Ag and therefore is considered as a micro-inclusion of electrum. In other case, gold peaks are not associated with detectable silver either by MPIXE or EPMA. Therefore, it may be suggested that these micro-areas represent accumulations of organic gold compounds.

The U-distribution analysed by MPIXE and EPMA is similar. It is most likely that U is present as micro-inclusions of thucholite, uraninite or brannerite in places were it correlates with Ti.

MPIXE also detected significant amounts of Zn, Zr, Rb and Bi in the clay organic matrix (Przybylowicz *et al.*, 1990).

The thucholite

Thucholite grains in shale are up to 4 mm in size, and the shale lamination around them is disturbed due to epigenetic growth. Thucholite is also present in boundary dolomite, a thin bed underlying black shale (Kucha, 1975, 1981, 1982) and in the top part of white sandstone (Banas *et al.*, 1978). The thucholite studied is hosted by boundary dolomite (Fig. 2*c*) and is free of microscopically visible inclusions of ore minerals (Fig. 2*d*), being composed of two optically distinct components: isotropic A, and anisotropic B.

Component A has a reflectivity in oil varying from 1.75 to 2.50%, with most values grouped close to the lower value. It is optically isotropic, homogeneous, free of microscopically visible ore minerals, with a higher content of heavy metals than the B component. As shown by TEM study the A component is amorphous.

Component B is strongly anisotropic in reflected light and is similar to graphite. It contains ubiquitous inclusions of uraninite, native gold, Pd-arsenides, Bi-sulphides and selenides, and brannerite. Electron diffraction study indicates the presence of three types of small-scale ordering (domains) in the anisotropic thucholite: (1) with

TABLE 2. Concentration of selected elements in the clay-organic matrix of the noble metal-bearing shale (ppm).

METHOD	BEAM SIZE (μm)	N	Ti	V	Fe	Ni	Cu	As	Mo	Pd	Ag	Pt	Au	U	
PIXE	3000	10	4400	2450	2200	90	2000	50	38	≤20	90		≤40	20	MIN
			29300	5700	32900	1400	51300	4900	1080	70	2500		700	3000	MAX
			13800	4000	10900	600	19400	1400	340	20	560		140	800	MEAN
MPIXE	3	13			5600	130	415	490	80	≤20	≤20	≤50	≤50	170	MIN
					8300	1400	7650	5300	540	≤20	40	≤50	150	2600	MAX
					7100	459	1587	1464	104	≤20	≤20	≤50	25	495	MEAN
EPMA	1	56	≤80	≤200	2700	≤200	≤60	≤200	≤100	≤200	≤300	≤360	≤100	≤500	MIN
			46100	4000	13900	1600	8800	3500	880	1900	1000	600	1900	11300	MAX
			3375	1100	9100	400	1950	1500	211	55	300	62	70	846	MEAN

N - number of analyses; ≤ - detection limit

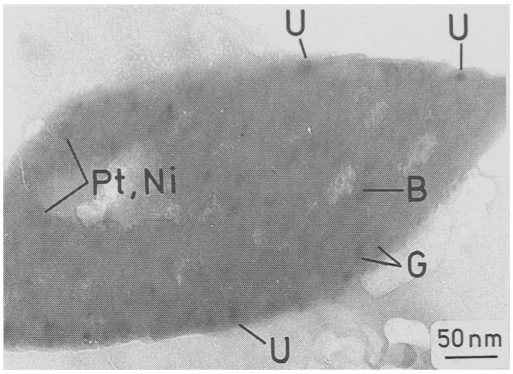

FIG. 3. TEM photomicrograph of thucholite with numerous inclusions of submicroscopic uraninite (U), brannerite (B), and diffuse inclusions of probable organometallic accumulations of gold (G) and organometallic accumulations of Pt–Ni.

typical graphite cell parameters $a_o = 0.246$ and $c_o = 0.672$ nm; (2) with Van der Waals thickness of the ring $a_o = 0.246$ and $c_o = 0.740$ nm; and (3) with a greater thickness of the ring where CH_3, CO or OH groups are attached to the conjugated benzene rings (Kucha and Wieczorek, 1988). The observed domains are smaller than 100 nm and cannot be resolved by XRD techniques. A strong optical anisotropy of thucholite arises from a large scale ordering of the three types of domains discussed above. The domains are oriented in such a way that their planes of conjugated benzene rings are always parallel, and therefore they form parallel clusters extending in size up to microscopic scale. This is responsible for a strong optical anisotropy similar to that of graphite.

Component A appears to be very inhomogeneous when studied under a high magnification TEM (Fig. 3). The matrix is full of finely dispersed inclusions with sizes from 0.004 to 0.025 μm. Two types of inclusion, one with sharp boundaries and the other with diffuse boundaries with the enclosing matrix can be distinguished. Energy-dispersive detector (EDS) measurements and a selected area diffraction study indicate that, in the first case, the inclusions are crystalline and consist of uraninite, brannerite and sometimes electrum, and, in the second case, the inclusions are amorphous and composed of organic U, Au or Ni–Pt compounds (Fig. 3). The chemical status of these amorphous, diffuse inclusions is not defined. Pt–Ni inclusions may be connected with pyrrole rings as suggested by a positive correlation between V, Ni and Pt.

The thucholite grain studied is embedded in Fe-dolomite (Fig. 2*c*). The major element present in thucholite is U, varying from ppm to a few wt.% (Table 3), which occurs as submicroscopic inclusions of UO_2, brannerite and probably some organometallic compounds (Fig. 3).

Chlorine and bromine are antipathetic in the studied profile (Fig. 2*c*), Cl being present at the edge and Br at the centre of the grain. However, a Br distribution should be considered with caution. Due to significant 'edge effects' on SXRFA scans, caused by penetration of the incident beam to *c.* 100 μm depth, when approaching the thucholite edge, more and more radiation comes from the underlying carbonate matrix free of Br. This produces a misleading distribution pattern. Similar, strong 'edge effects' are seen in the case of Fe and Mn as well as Pb and Bi. An increased content of Fe and Mn is seen at the edge of the thucholite grain and most certainly comes from the underlying carbonate matrix rich in both Fe

TABLE 3. Concentration of selected elements in the thucholite matrix free of microscopically visible ore minerals (ppm).

METHOD	BEAM SIZE (μm)	N	Ti	V	Fe	Ni	Cu	As	Mo	Pd	Ag	Pt	Au	Pb	U	
PIXE	3000	25	120	120	2200	≤7	300	11	≤8	≤12	≤18	≤13	≤13	≤18	≤35	MIN
			5900	460	28700	900	93700	600	170	100	100	≤13	800	6400	38000	MAX
			1084	172	10620	220	23780	292	67	26	28	≤13	35	1400	19600	MEAN
MPIXE	3	11			140	≤17	130	≤10	≤50	≤110	≤100	≤33	≤33	50	12000	MIN
					5800	180	5560	1280	160	310	≤100	270	≤33	3700	68000	MAX
					1107	45	355	332	30	28	≤100	29	≤33	593	44800	MEAN
SXRFA	15x20	21			73	≤5	1300	5				≤2	≤1	≤3		MIN
					1300	650	5000	5100				1770	1900	490		MAX
					396	67	2207	1432				162	175	215		MEAN
EPMA	1	27	≤130	≤300	≤200	≤150	≤200	≤100		≤300	≤300	≤200	≤300	≤600	≤400	MIN
			1420	2200	2200	500	1800	5000		5000	3900	2100	800	1400	162400	MAX
			620	504	390	109	510	270		390	504+	480	291+	410	28600	MEAN

+ - native inclusions excluded; ≤ - detection limit

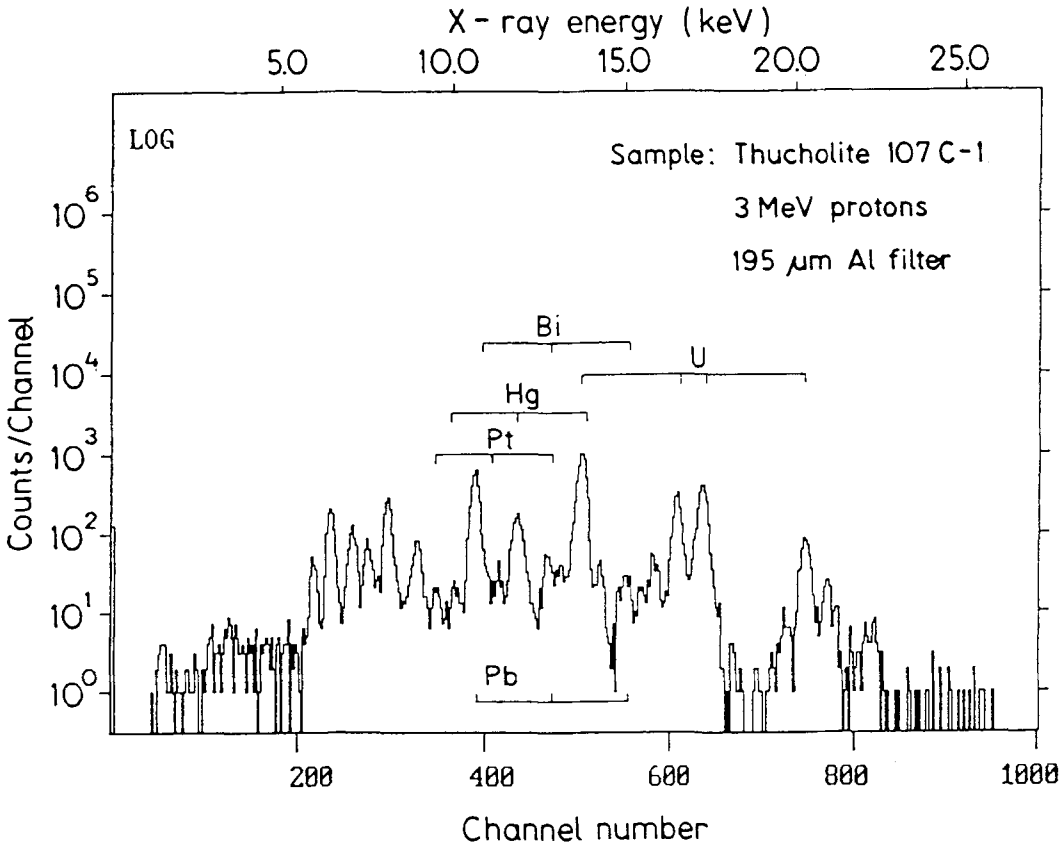

FIG. 4. X-ray spectrum of thucholite showing lines of Pt, Hg and Bi. The main overlapping elements U and Pb are also shown. Spectrum was obtained with MPIXE.

and Mn. The 'edge effect' is not observed on EPMA runs, except of two Fe determinations set at the very edge of the grain. This is connected with a very shallow penetration of the EPMA beam, in the thucholite from a few to 12 μm depending on the uranium content in a given area. Bi and Pb are connected with the thucholite matrix and they gradually disappear towards the edge of the grain.

A distribution of noble metals determined by SXRFA and EPMA is difficult to correlate due to very different detection limits (Table 3), beam spot size and beam penetration depth. In general, correlations between elements determined with SXRFA and with EPMA are similar. In a majority of the studied micro-areas, analysed elements were detected by both methods, although the measured quantities are usually different. This relationship is best illustrated by gold. There were three subsurface micro-inclusions of electrum detected by SXRFA (1.2, 1.2 and 4.0 wt.% of Au respectively), but only one of these has been reached by the electron beam of EPMA (3.3 wt.% of Au, 1.7 wt.% of Ag). The other two subsurface micro-inclusions of electrum are too deep to be reached by an electron beam of EPMA.

Conclusions regarding detection limits

To improve detection of noble metals on EPMA a counting time of 40 sec was used for peak and background. Background was measured on both sides of the peak. To define minimum detection limit (MDL), the 3δ rule was applied (Ziebold, 1967). The MDLs of EPMA measurements are shown in Table 2 and 3 and vary from 100 to 500 ppm.

The PIXE and MPIXE MDLs were calculated using a software package developed for thick targets (Kajfosz, 1987) based on assumptions used by Currie (1968): $C = 3.29\delta$, where δ is the

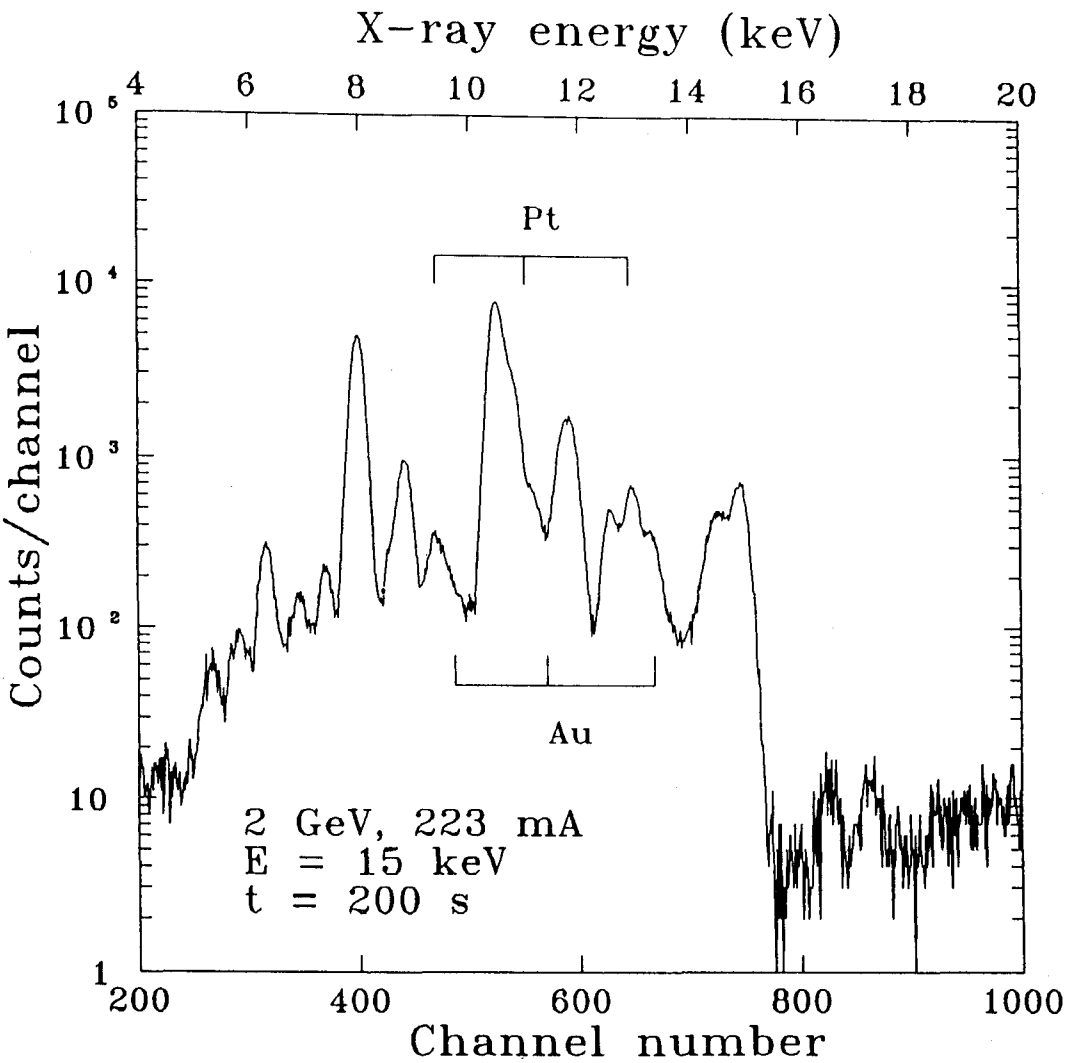

FIG. 5. SXRFA emission spectrum of thucholite obtained with 15 keV beam. A lack of overlapping U and Pb lines permits a clear distinguishing of Pt and Au.

standard deviation of background defined in an energy interval equal to double the full width at half-maximum, centred at the expected Kα or Lα peak position (Przybylowicz *et al.*, 1990). Depending on the studied target and analysed element, the PIXE and MPIXE MDLs vary from 8 to 110 ppm. The main factor responsible for difficulties in obtaining detection limits at the ppm level was an increased U and, to a minor extent, an increased Pb content (Przybylowicz *et al.*, 1990). For example Pt, Hg and Bi peaks appear close to U lines (Fig. 4) and therefore an increasing U content obscures the spectra and worsens detection limits. Moreover, during analysis of micro-areas rich in U the beam current cannot be kept as high as for U-free micro-areas due to large pile-up peaks of X-ray spectra, and lowering the incident beam intensity means decreasing the MDLs (Przybylowicz *et al.*, 1990).

The SXRFA MDLs are lower than is the case for PIXE and MPIXE (Table 3) because of fewer overlapping U lines excited by the 15 keV incident beam. Clear resolution of Lα lines of Au and Pt in the thucholite matrix (Fig. 5) is possible when the X-ray emission spectra do not contain

interfering U lines. The SXRFA detection limits are from 1 to a few ppm (Table 3).

Acknowledgements

We are grateful to Dr. C. J. Stanley of the Natural History Museum, London, for grammatical improvements to the manuscript.

References

Banas, M., Jarosz, J., and Salamon, W. (1978) *Mineral. Pol.*, **9**, 3–21.

Campbell, J. L., and Coockson, J. A. (1984) *Nucl. Instr. and Meth.*, **B3**, 185–97.

Campbell, J. L., Perujo, A., Teesdale, W. J., and Coockson, J. A. (1988) Ibid. **B30**, 317–23.

Currie, L. A. (1968) *Anal. Chem.*, **40**, 586–593.

Kajfosz, J. (1987) *Int. Rep. of the Lab. of Applied Nuclear Spectroscopy*. Institute of Nuclear Physics, Krakov, Poland (in Polish).

Kajfosz, J. and Kwiatek, W. M. (1987) *Nucl. Instr. and Meth.*, **B22**, 78–81.

Kopp, O. C., Reeves, D. K., Rivers, M. L., and Smith, J. V. (1990) *Chem. Geol.*, **81**, 337–47.

Kucha, H. (1975) *Mineral. Pol.*, **6**, 87–92.

—— (1976) *Ann. Soc. Geol. Pol.*, **46**, 369–417.

—— (1981) *Tschermak's Min. Petr. Mitt.*, **28**, 1–16.

—— (1982) *Econ. Geol.*, **77**, 1578–91.

—— (1983) *Trans. Instn Min. Metall.*, **92**, B72–B79.

—— (1984) *Chemie Erde*, **43**, 27–43.

—— (1985) *Trans. Instn Min. Metall.*, **94**, B133–46.

—— (1990) *Geologische Rundschau*, **79**, 387–99.

—— Mayer, W., and Piestrzynski, A. (1983) *Mineral. Pol.*, **14**, 35–43.

—— and Wieczorek, A. (1988) *Mineral. Deposita*, **23**, 174–8.

Piestrzynski, A. (1990) Ibid., **25**, 146–51.

Przybylowicz, W., Kucha, H., Kajfosz, J and Szymczyk, S. (1989) *Proc. 12th Int. Conf. on X-ray Optics and Microanalysis*, Krakov, Poland (Ed. S. Jasienska), 929pp.

—— —— H., Pietrzynski, A., Traxel, K., and Bajt, S. (1990) *Nucl. Instr. and Meth.*, **B50**, 231–7.

—— Langevelde Van, F., Kucha, H., Lankosz, M., and Wyszomirski, P. (1992) *Nucl. Instr. and Meth.*, **B68**, 115–21.

Remond, G., Cesbron, F., Traxel, K., Campbell, J. L., and Cabri, L. J. (1987) *Scanning Microscopy*, **1**, 1017–23.

Salamon, W. (1979) *Mineral. Trans. Acad. Pol. Sci.*, **62**, 59 pp. (in Polish).

Sawlowicz, Z. (1985) *Mineral. Pol.*, **16**, 35–42.

Ziebold, T. (1967) *Anal. Chem.*, **39**, 858–61.

[*Manuscript received 15 April 1992*]